TOWARD AN ADVANCED INFORMATIONAL FRAMEWORK FOR IMPROVING MINIMALISTIC VISUAL ODOMETRY

J. AL HAGE [(1)], S. MAFRICA [(2,3)], M. EL BADAOUI EL NAJJAR [(1)], F. RUFFIER [(2)]
joelle.al-hage@ed.univ-lille1.fr, stefano.mafrica@mpsa.com, maan.e-elnajjar@univ-lille1.fr, franck.ruffier@univ-amu.fr
[(1)] CRIStAL laboratory CNRS UMR 9189, University of Lille, 59650 Villeneuve d'Ascq, France
[(2)] Aix Marseille Univ, CNRS, ISM, Marseille 13009, France
[(3)] PSA Peugeot Citroën, 78140 Vélizy-Villacoublay, France

ABSTRACT

On the planet Mars, assessing the trajectory and the odometry onboard an exploratory rover safely in real time is an imperative because of the sandy composition of most of the soil. To obtain an accurate self-localization method for use in this context, a data fusion method was developed based on minimalistic bio-inspired Optic Flow (OF) sensors and an Inertial Measurement Unit (IMU). However, in this environment, errors of various kinds are liable to affect the sensors' measurements and thus decrease the accuracy of the localization estimates. A Fault Detection and Exclusion (FDE) step was therefore added, which greatly improved the robot's odometric performances.

In this study, an informational framework for fault tolerant data fusion is presented and the validity of this approach was confirmed by the experimental data obtained in tests performed on a car-like robot in both indoor and outdoor environments.

1. INTRODUCTION

Long distance navigation in unknown environments requires an accurate positioning method. The localization integrity is therefore a key factor in planetary rover operations [1][2][3][4] in which it is proposed to explore the area in order to determine whether it contains any signs of life or to assess the geological and climatic features.

Visual odometry techniques based on motion tracking between two consecutive images have proved to be effective means of localizing a rover on Mars [5] [6]. However, solutions based on the use of a standard camera have disadvantages such as the high computational cost of the image processing and the inability of these methods to cope with a large dynamic range of light conditions. In this study based on a visual odometry approach, novel bio-inspired OF sensors were used. In a previous study [7], these sensors have allowed an accurate measurements in a large dynamic range of lighting conditions as well as during exposure to vibration.

Data fusion between the OF and IMU measurements was achieved using the informational version of the Kalman Filter (KF), namely the Information Filter (IF). With the KF, the inversion of a matrix having the dimension of the observation vector is performed, whereas the IF inverses a matrix having the dimension of the state vector. The IF update step is also modelled by simply summing the various information contributions from different observations which makes this filter suitable for real time applications and for dealing with multi-sensor data fusion situations [8].

In planetary rover operations conducted in completely or practically unknown environments, various errors are liable to affect the sensors' measurements and thus reduce the integrity and the accuracy of the localization estimates. Detecting and excluding errors in the measurements is a crucial means of improving the integrity of a rover's positioning performances.

The informational framework adopted here in the FDE step was based on the use of a bank of Extended IFs (EIFs) and information theory tools. Comparison between the data distribution obtained in the update step of the EIF (by combining OF and IMU) with that obtained in the prediction step (using the dynamic model) allows the detection of fault. This comparison was made by calculating the Kullback-Leibler Divergence (KLD) between the *a priori* and *a posteriori* distributions of the EIF. To exclude the errors from the fusion procedure, a bank of EIF_j was generated and a set of residuals based on the KLD was developed. Each residual (KL^j) takes into account the information contribution of one measurements (z_j). The measurement giving the maximum KL^j value is then removed from the fusion procedure. This procedure is repeated iteratively until no errors are detected any longer. Note that the modelling of the IF update step facilitates the implementation of the FDE step.

This paper is organised as follows: the method used to combine the OF and IMU measurements using the EIF is presented in Section 2. The FDE approach based on informational procedure is presented in Section 3. Results obtained using real experimental data on a car-like robot in both indoor and outdoor environments are presented in section 4, followed by the authors' conclusions in section 5.

2. IMU/OPTIC FLOW DATA FUSION BASED ON THE INFORMATION FILTER

In this study, we focused on a car-like robot (Figure 1) driven by a DC motor and equipped with 2 downward-facing 12-pixel Optic Flow (OF) sensors [7] (one on the left and the other on the right) as well an Inertial Measurement Unit (IMU). This robot estimates its own velocity and steering angle, and therefore its position and orientation, based on the following informational approach.

The state vector of the robot taken to be the longitudinal velocity V and the steering angle $\emptyset$ is denoted: $\xi = [V, \emptyset]^T$

In order to estimate the robot's state vector, an Extended Information Filter (EIF) is applied which it is divided into two steps:

- Prediction where the dynamics of V and $\emptyset$ are obtained from a model (previously identified using the ground-truth measurements),
- update where the OF and the IMU measurements are used in order to correct the prediction.

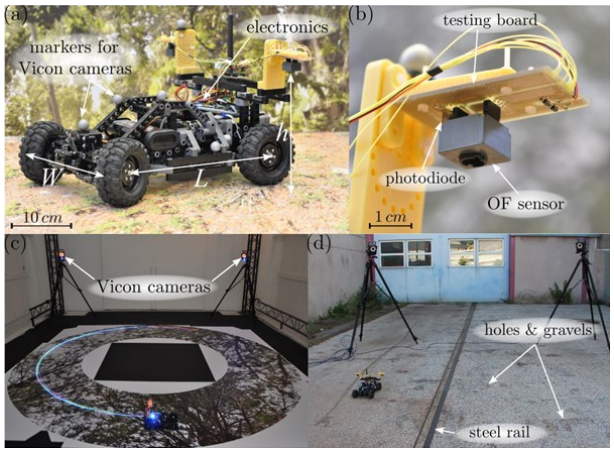

Figure 1. The low-cost car-like robot called BioCarBot. (b) One of the two OF sensors used on the robot. (c) The indoor test environment equipped with Vicon cameras. (d) The outdoor test environment equipped with Vicon cameras. The ground, which consisted mainly of asphalt, included holes, gravel and a steel rail. From [7].

2.1. Prediction step

The dynamics of V and $\emptyset$ were identified in the following form [7]:

$$\xi_{k+1} = \xi_k + [A\,\xi_k + B\,u_k]T_e \qquad (1)$$

where:
k is the sampling instant
$A = \text{diag}\,(a_1, a_2), B = \text{diag}\,(b_1, b_2)$
$a_1 = -b_1 = -2.15$, $a_2 = -b_2 = -4.87$
u is the input vector obtained from the control inputs.
T_e is the sampling period.

The covariance matrix is written as follows:

$$P_{k+1/k} = F_k\,P_{k/k}F_k^T + Q \qquad (2)$$

where:

$$F_k = I_{2\times2} + A\,T_e \qquad (3)$$

and Q is the covariance matrix associated to the process state noise, which is taken to be white Gaussian noise with a zero mean.

Since the estimator is the IF, the information matrix and the information vector have to be calculated: these are expressed in equations (4) and (5), respectively [9]:

$$Y_{k+1/k} = P_{k+1/k}^{-1} \qquad (4)$$

$$y_{k+1/k} = Y_{k+1/k}\,\xi_{k+1/k} \qquad (5)$$

2.2. Update

In order to reduce the uncertainty of the dynamic model, the OF and IMU measurements are combined using the IF.
The OF measured between the i-1-th and the i-th pixels is denoted by ω_i and modelled as follows:

$$z_i = \begin{pmatrix}\omega_i^l\\ \omega_i^r\end{pmatrix} = h_i(k) = \begin{pmatrix}\dfrac{(L - y_l\tan\emptyset)\sin^2\varphi_i^l}{hL}\\ \dfrac{(L - y_r\tan\emptyset)\sin^2\varphi_i^r}{hL}\end{pmatrix}V \qquad (6)$$

where:
ω_i^l and ω_i^r are the i-th OFs delivered by the left and right sensors, respectively,
φ_i^l and φ_i^r are the orientations of the pixel's axis corresponding to the OF values ω_i^l and ω_i^r.
L(=255mm) is the distance between the rear and front wheel axes,
y_l =-y_r(=140mm) are the y-values of the left and right OF sensors with respect to the body frame <B> placed in the middle of the rear wheel axis.
h is the height of the OF sensors above the ground.

Since the observation model is non-linear, the EIF is applied and the Jacobian matrix $H_i = \frac{\partial h_i}{\partial \xi}\Big|_{\xi_{k/k-1}}$ is computed:

$$H_i = \begin{pmatrix}\dfrac{(L - y_l\tan\emptyset)\sin^2\varphi_i^l}{hL} & \dfrac{-y_l\sin^2\varphi_i^l(1+\tan^2\emptyset)V}{hL}\\ \dfrac{(L - y_r\tan\emptyset)\sin^2\varphi_i^r}{hL} & \dfrac{-y_r\sin^2\varphi_i^r(1+\tan^2\emptyset)V}{hL}\end{pmatrix} \qquad (7)$$

The noise associated with the OF measurements is assumed to be white Gaussian noise with a zero mean and the covariance matrix is written R=diag(σ_l^2, σ_r^2).

On the other hand, the output model corresponding to the IMU measurements is given by:

$$z_{IMU} = \begin{pmatrix} a_x \\ \Omega_z \\ \Omega_{DC} \end{pmatrix} = h_{IMU}(k) \approx \begin{pmatrix} a_1 V + b_1 u_1 + g \sin \beta_{IMU} \\ \frac{\tan \emptyset}{L} V \\ \frac{k_g}{2\pi r} V \end{pmatrix} \quad (8)$$

where Ω_z is the angular velocity obtained in terms of the Ackermann steering geometry [10], a_x is the linear acceleration on the *x*-axis, Ω_{DC} is the DC motor's speed, g is the gravity acceleration, *r* (=14mm) is the radius of the robot's wheel, $k_g (= 3.4)$ is the transmission gear ratio and β_{IMU} is the angle giving the rotation about the *y*-axis between the body frame <B> and the inertial frame <I>. Note that in the inertial frame, the *x*- and *y*-axes lie on the local ground plane (for further details, see [7]).

The observation matrix H_{IMU} associated with the IMU observation model can be written as follows:

$$H_{IMU} = \begin{pmatrix} a_1 & 0 \\ \frac{\tan \emptyset}{L} & \frac{V}{L}(1 + \tan^2 \emptyset) \\ \frac{k_g}{2\pi r} & 0 \end{pmatrix} \quad (9)$$

The noise associated with the IMU observations is assumed to be white Gaussian noise with a zero mean and covariance matrix R_{IMU}=diag(0.263^2,0.047^2,0.001^2).

The information matrix and the information vector are updated as follows:

$$Y_{k/k} = Y_{k/k-1} + \sum_{j=1}^{N} I_j(k) \quad (10)$$

$$y_{k/k} = y_{k/k-1} + \sum_{j=1}^{N} i_j(k) \quad (11)$$

where *N* is the number of observations and $(I_j(k), i_j(k))$ are the information contributions from the observation z_j ($z_j = [\omega_j^l \; \omega_j^r]^T$ or $z_j = z_{IMU}$):

$$I_j(k) = H_{j,k}^T R_j^{-1}(k) H_{j,k} \quad (12)$$

$$i_j(k) = H_{j,k}^T R_j^{-1}(k) \left[\left(z_{j,k} - z_{j,estimate} \right) + H_{j,k} \xi_{k/k-1} \right] \quad (13)$$

$H_{j,k}$ and $z_{j,estimate}$ are given in equations (7) and (6), respectively, in the case of the OF measurements and in equations (9) and (8) in that of the IMU measurements.

It is worth noting that the main advantage of the EIF involves the update step, where it is modelled as a simple sum of the information contributions of the various observations. This formula lends itself well to real time applications, especially when the number of observations is greater than the dimension of the state vector [11].

The absolute robot's position ($[x, y]$) and orientation θ are obtained from the Ackermann model [10], using the EIF estimate ξ_k as an input.

3. FAULT DETECTION AND EXCLUSION METHOD BASED ON KULLBACK-LEIBLER DIVERGENCE

Errors of various kinds are liable to affect the IMU and OF measurements and thus decrease the robot's localization integrity. These errors therefore have to be detected and eliminated from the fusion procedure.

In this study, a residual based on the KLD [12] [13] between the *a priori* Gaussian probability distribution ($g(k/k-1)$) based on the dynamic model and *a posteriori* Gaussian probability distribution ($g(k/k)$) obtained from the update step of the EIF is computed. This residual is denoted *GKLD* (Global Kullback-Leibler Divergence) and can be expressed as follows [9]:

$$GKLD = KLD(g(k/k-1) || g(k/k)) = \frac{1}{2} trace\left(Y_{k/k} \; Y_{k/k-1}^{-1}\right) + \frac{1}{2} \log \frac{|Y_{k/k-1}|}{|Y_{k/k}|} - \frac{1}{2} M + \frac{1}{2} \left(\xi_{k/k} - \xi_{k/k-1}\right)^T Y_{k/k} \left(\xi_{k/k} - \xi_{k/k-1}\right) \quad (14)$$

where *M* is the dimension of the state vector (*M*=2).

The *GKLD* allows two types of tests [9]:

- Test on the means of the data distributions obtained using the Mahalanobis distances: $\left(\xi_{k/k} - \xi_{k/k-1}\right)^T Y_{k/k} \left(\xi_{k/k} - \xi_{k/k-1}\right)$,
- Test on the covariance matrices obtained using Burg matrix divergence [14]: $trace\left(Y_{k/k} \; Y_{k/k-1}^{-1}\right) + \log \frac{|Y_{k/k-1}|}{|Y_{k/k}|} - M$.

In the fault-free case, the general distribution of the *GKLD* is related to the Chi-square and Fisher distributions [9] as follows:

$$GKLD \sim \frac{1}{2} \left[\frac{M(n-1)}{(n-M)n} F_{M,n-M} + \frac{1}{n-1} \frac{1}{1 - \frac{1}{6(n-1)-1}\left(2M+1-\frac{2}{M+1}\right)} \chi^2_{\frac{1}{2}(M(M+1))} \right] \quad (15)$$

where *n* is the number of samples.

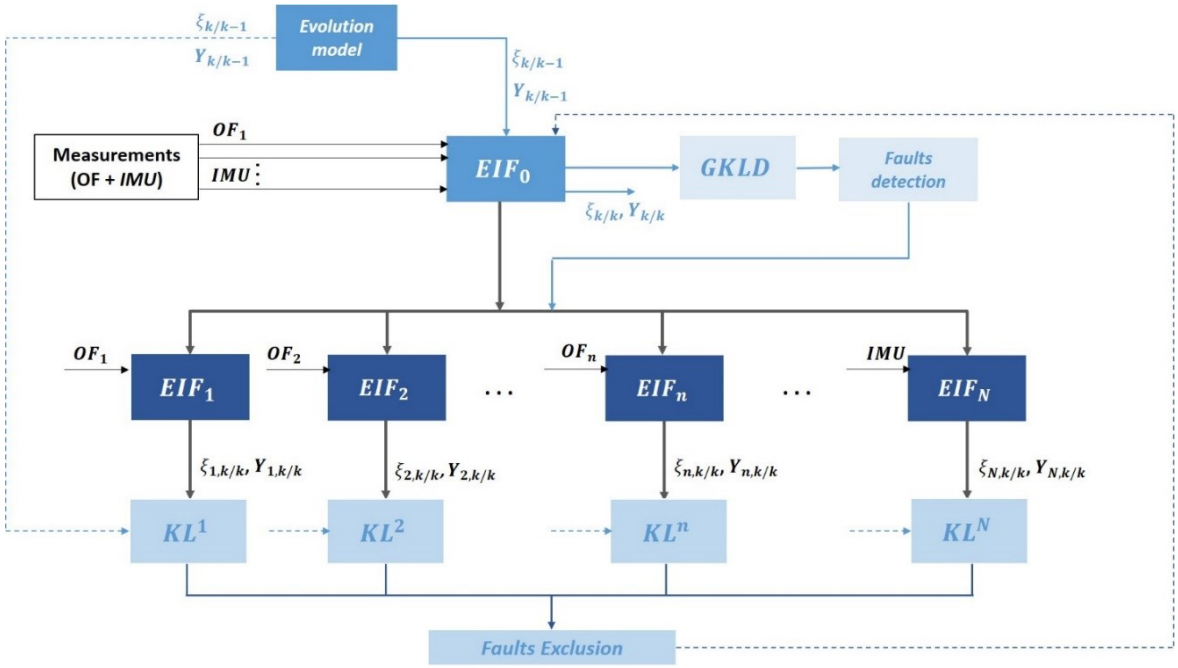

Figure 2. The data fusion approach used here, including the FDE step.

In order to exclude measurement errors, a bank of EIFs was designed (EIF_j) and a set of residual based on the KLD is developed. Each residual, denoted KL^j, takes into account the information contribution of one observation z_j. KL^j gives the divergence between the predicted distribution and the updated distribution obtained after combining the measurement z_j. The observation giving the maximum value of KL^j is removed from the fusion procedure. This procedure is repeated iteratively until no faults are detected any longer using the *GKLD* residual test (Figure 2).

The residual KL^j is expressed in the form:

$$KL_k^j = \frac{1}{2} trace(Y_{j\,k/k}\, Y_{k/k-1}^{-1}) + \frac{1}{2}\log\frac{|Y_{k/k-1}|}{|Y_{j\,k/k}|} - \frac{1}{2}M + \frac{1}{2}\left[(\xi_{j\,k/k} - \xi_{k/k-1})^T Y_{j\,k/k}(\xi_{j\,k/k} - \xi_{k/k-1})\right] \quad (16)$$

where:

$$Y_{j\,k/k} = Y_{k/k-1} + I_j(k) \quad (17)$$

$$y_{j\,k/k} = y_{k/k-1} + i_j(k) \quad (18)$$

$$\xi_{j\,k/k} = (Y_{j\,k/k})^{-1} y_{j\,k/k} \quad (19)$$

4. EXPERIMENTS AND VALIDATION OF THE RESULTS

Figure 1 shows pictures of the BioCarBot robot, one of the two OF sensors used and the indoor and outdoor test environments equipped with a Vicon motion-capture system. The odometric method developed here was tested using a car-like robot based on the 2WD Racecar Kit provided by Minds-I Robotics, which was chosen despite the low resolution of the servo and motor control systems. Thanks to the modularity of the robot's structure, two identical OF sensors giving 10 raw downward-facing measurements on the right of the robot and 10 raw downward-facing measurements on the left (which have also been called VMSs [7],[15]) were attached to the robot's frame on both sides, aligned with the rear wheel axis (Figure 1a). To obtain ground-truth values, the robot's 3-D pose was measured with a Vicon motion-capture system via the infrared markers attached to the robot's frame (Figure 1a). Indoor experiments were performed in the Marseille flying arena, whereas four individual Vicon cameras, each mounted on a tripod, were used in the outdoor experiments (Figures 1c and 1d). The robot was driven in a closed-loop mode based on the estimates of the velocity and steering angle values. IMU and OF sensor data were reused in batch mode to assess the robot's odometric performances based on the present informational framework.

The first test was conducted in the indoor environment, where the robot was driven along a path forming a figure of eight (Figure 5).

Figure 3a presents the *GKLD* residual used to quantify the divergence between the predicted and updated distributions of the EIF. After filter convergence was reached, the jumps visible on the

GKLD indicate the presence of measurement errors. These errors had to be excluded from the fusion procedure. For this purpose, the set of residuals KL^j was calculated in order to quantify the information contributions of each measurement z_j (Figure 3b). The observation (z_j) giving the maximum value of KL^j was removed from the fusion procedure. In this test, the errors detected occurred mainly in the OF measurements.

The longitudinal velocity V and the steering angle $\emptyset$ estimated after the FDE step (based on the raw OF data combined with the IMU measurements) are presented versus the ground truth values in Figure 4. Likewise, the estimated trajectory after applying the informational framework is compared with the ground truth trajectory in Figure 5.

The errors observed in the absolute position and orientation estimates before and after the FDE step are given in Figure 6. The mean value of the errors amounted to about 0.3039 m in the position and 0.1238 rad in the orientation before the FDE step. After the fault exclusion procedure, the mean errors dropped to 0.2873 m in the position and 0.1103 rad in the orientation.

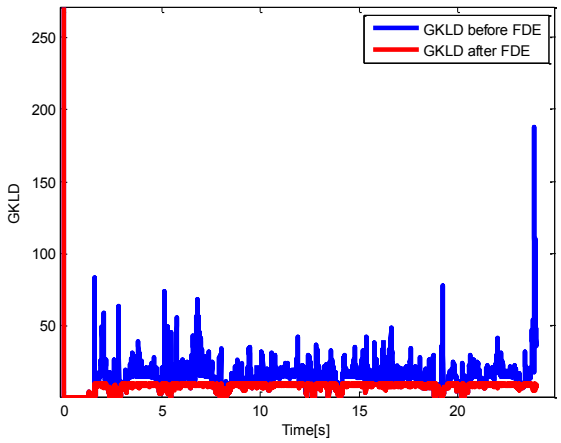

(a) The *GKLD* used for faults detection

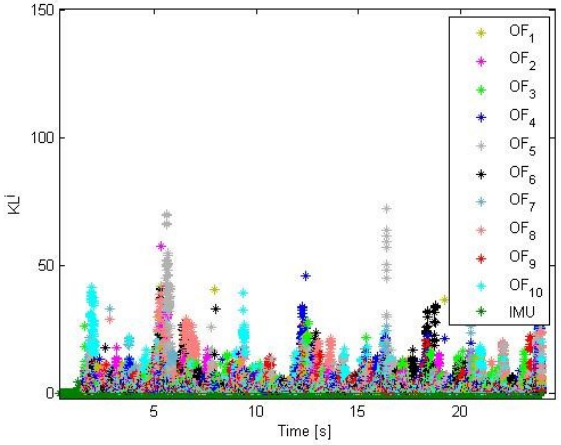

(b) The residual set KL^j used for faults exclusion

Figure 3. The FDE step.

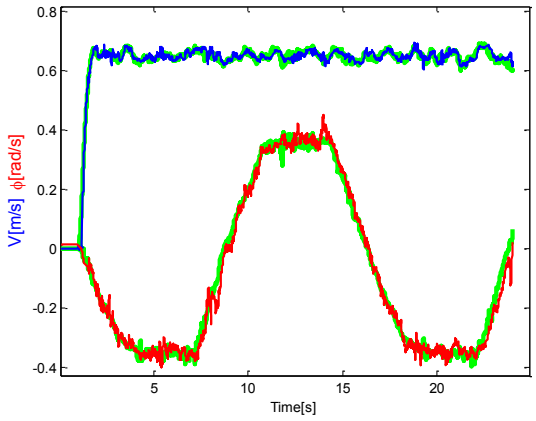

Figure 4. The values of V and $\emptyset$ obtained using the present informational framework (in blue and red) in comparison with the ground truth values (in green).

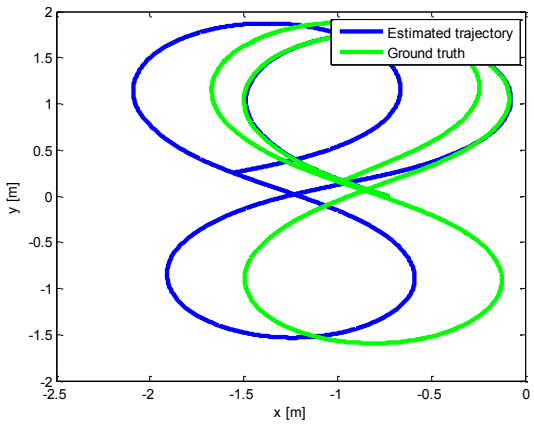

Figure 5. The trajectory estimated after the FDE step.

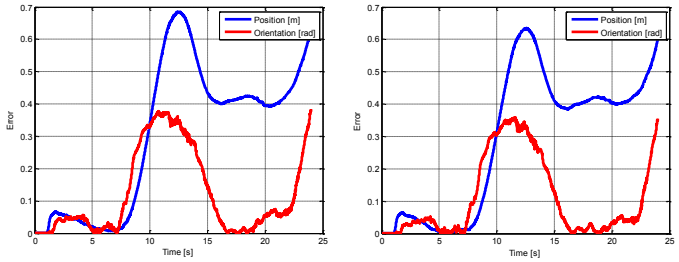

(a) Before the FDE step (b) After the FDE step

Figure 6. Errors in the position and orientation.

Another test was carried out in the outdoor environment in the presence of a recurrent vertical vibratory disturbance caused by a steel rail placed across the robot's circular path (figure 9b).

The *GKLD* used to detect errors is shown in Figure 7, where the many jumps visible indicate the ability of the residual to detect the presence of the perturbations generated. Once a measurement error has been detected, it has to be excluded from the fusion procedure. The set of residuals KL^j was therefore determined as shown in Figure 8 in order to compute the information contribution of each measurement. Contrary to the test conducted in the indoor environment, it can be seen from Figure 8 that the IMU measurements gave the maximum value of the KL^j, which meant that these measurements had to be removed from the fusion procedure.

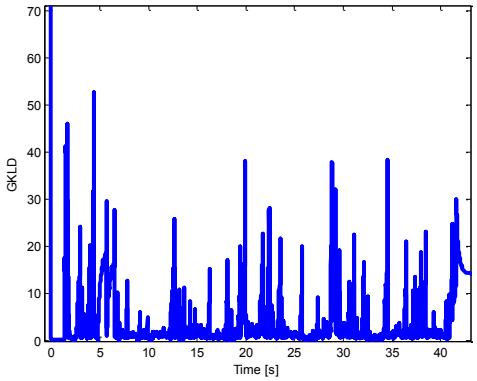

Figure 7. The *GKLD* used for faults detection.

The values of the estimated state vector and the estimated trajectory obtained after the FDE step are presented in Figure 9 a and b, respectively, in comparison with the ground truth values. The errors in the position and the orientation observed before and after the FDE step are shown in Figure 10. This step therefore improved the error values, since the mean position error, which was about 1.7256 m before the FDE step, decreased to about 0.7321m after the FDE step. Likewise, the orientation error, which was about 1.932 rad before the FDE step, decreased to 0.5468 rad after the FDE step.

The experiments conducted in the outdoor environment in the presence of vibratory perturbations proved the efficiency of the present informational framework as a means of detecting and excluding the faulty measurements from the fusion procedure, which greatly improved the robot's positioning performances. Likewise, this test shows the value of the OF sensors and their robustness to disturbances, which was greater than that of the IMU measurements.

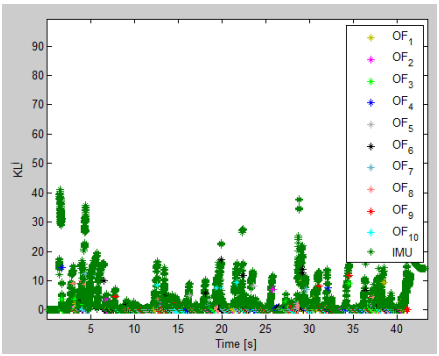

Figure 8. The set of residuals KL^j used for the faults exclusion.

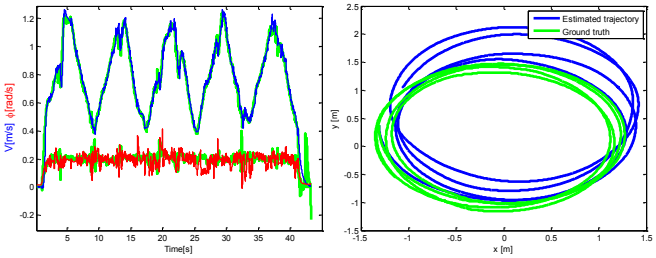

(a) The estimated value of V and $\emptyset$ (in blue and red), versus the ground truth values (in green)

(b) The estimated versus ground truth trajectory

Figure 9. Estimations versus ground truth values.

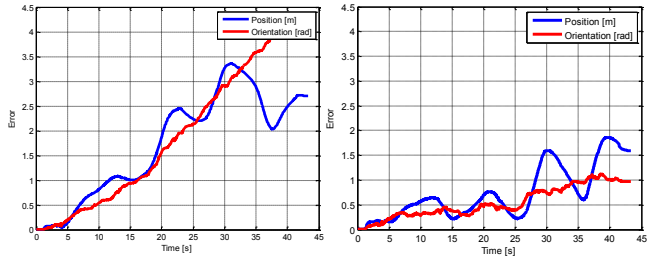

(a) Before the FDE step (b) After the FDE step

Figure 10. Errors observed in the position and orientation estimates before and after the FDE step.

5. CONCLUSION

In this paper, an informational procedure is presented for improving robots' minimalistic visual odometric performances. This framework is based on the use of EIF for combining the IMU and OF raw data, and the *GKLD* for detecting measurement errors. A bank of EIFs was generated and a set of residuals was computed in order to exclude the erroneous measurements from the fusion procedure.

Experimental results obtained in both indoor and outdoor environments show the efficiency of this procedure based on an informational framework and an FDE step as a means of improving the robot's localization accuracy. In particular, the elegant method presented here for fusing IMU and OF measurements and automatically rejecting any IMU measurements which were strongly affected by the vibratory disturbance greatly improved the robot's odometry performances. The approach presented here is suitable for real time applications because adding or removing an observation will affect only the number of additions required to correct the state estimates.

6. REFERENCES

[1] T. M. Howard *et al.*, "Enabling continuous planetary rover navigation through FPGA stereo and visual odometry," in *Aerospace Conference, 2012 IEEE*, 2012, pp. 1–9.

[2] A. Howard, "Real-time stereo visual odometry for autonomous ground vehicles," in *Intelligent Robots and Systems, 2008. IROS 2008. IEEE/RSJ International Conference on*, 2008, pp. 3946–3952.

[3] A. E. Johnson, S. B. Goldberg, Y. Cheng, and L. H. Matthies, "Robust and efficient stereo feature tracking for visual odometry," in *Robotics and Automation, 2008. ICRA 2008. IEEE International Conference on*, 2008, pp. 39–46.

[4] Y. Cheng, M. Maimone, and L. Matthies, "Visual odometry on the Mars exploration rovers," in *Systems, Man and Cybernetics, 2005 IEEE International Conference on*, 2005, vol. 1, pp. 903–910.

[5] D. M. Helmick, Y. Cheng, D. S. Clouse, L. H. Matthies, and S. I. Roumeliotis, "Path following using visual odometry for a mars rover in high-slip environments," in *Aerospace Conference, 2004. Proceedings. 2004 IEEE*, 2004, vol. 2, pp. 772–789.

[6] M. Maimone, Y. Cheng, and L. Matthies, "Two years of visual odometry on the mars exploration rovers," *J. Field Robot.*, vol. 24, no. 3, pp. 169–186, 2007.

[7] S. Mafrica, A. Servel, and F. Ruffier, "Minimalistic optic flow sensors applied to indoor and outdoor visual guidance and odometry on a car-like robot," *Bioinspir. Biomim.*, vol. 11, no. 6, p. 066007, 2016.

[8] H. Durrant-Whyte, *Introduction to decentralised data fusion*. The University of Sydney, Sydney, Australia, 2004.

[9] J. Al Hage, M. E. El Najjar, and D. Pomorski, "Multi-sensor fusion approach with fault detection and exclusion based on the Kullback–Leibler Divergence: Application on collaborative multi-robot system," *Inf. Fusion*, vol. 37, pp. 61–76, Sep. 2017.

[10] A. De Luca, G. Oriolo, and C. Samson, "Feedback control of a nonholonomic car-like robot," *Robot Motion Plan. Control*, pp. 171–253, 1998.

[11] N. Assimakis, M. Adam, and A. Douladiris, "Information filter and kalman filter comparison: Selection of the faster filter," *Int. J. Inf. Eng.*, vol. 2, no. 1, pp. 1–5, 2012.

[12] S. Kullback, *Information theory and statistics*. Courier Corporation, 1968.

[13] J. V. Davis and I. S. Dhillon, "Differential Entropic Clustering of Multivariate Gaussians," in *Neural information processing systems (NIPS)*, 2006, pp. 337–344.

[14] B. Kulis, M. Sustik, and I. Dhillon, "Learning low-rank kernel matrices," in *Proceedings of the 23rd international conference on Machine learning*, 2006, pp. 505–512.

[15] F. Roubieu, F. Expert, G. Sabiron, and F. Ruffier, "A two-directional 1-gram visual motion sensor inspired by the fly's eye," *IEEE Sens. J.*, vol. 13, no. 3, pp. 1025–1035, 2013.